- 1 Electrochemically Active Surface Area Controls HER Activity for Fe_xNi_{100-x} Films in
- 2 Alkaline Electrolyte
- 3 Sergio I. Perez Bakovic^a, Prashant Acharya^a, Morgan Watkins^a, Hannah Thornton^a, Shixuan Hou^a,
- 4 and Lauren F. Greenlee*, a
- 5 aRalph E. Martin Department of Chemical Engineering, University of Arkansas, Fayetteville, AR
- 6 72701, United States
- 7 *Corresponding author: 3202 Bell Engineering Center, Ralph E. Martin Dept of Chemical
- 8 Engineering, University of Arkansas, Fayetteville, AR 72701; greenlee@uark.edu

9 Abstract

10

11

12

13

14

15

16

17

18

19

20

The synthesis and electrocatalytic activity of Fe_xNi_{100-x} electrochemically deposited films were investigated. Films were evaluated for the hydrogen evolution reaction (HER) in alkaline media with respect to composition and electrochemically active surface area (ECSA). Results demonstrate that films of higher or equal Fe content had an ECSA tenfold greater than films with higher Ni. When normalized by geometric surface area, Fe₅₀Ni₅₀ films required the lowest overpotential of -390 mV to reach a current density of -10 mA cm⁻². However, when normalized by the ECSA, intrinsic HER activity increases as Ni content increases. Tafel slope, ECSA, microscopy, and impedance spectroscopy analyses allow a decoupled analysis of surface area versus activity effects on overall measured HER activity. These analyses collectively demonstrate that the increase in electrocatalytic activity is attributed to the increase in ECSA and not to an enhancement in the intrinsic activity by Fe and Ni component interactions.

21 **Keywords:** electrodeposition, iron, nickel, films, alkaline, hydrogen evolution reaction, electrochemically active surface area, intrinsic activity.

23

24

25

26

27

28

29

30

31

32

33

34

35

36

37

38

39

40

41

1. Introduction

The conversion of renewable energy (solar and wind) to electrical energy has increased, nearly doubling from 2008 to 2018 in the United States [1]. As a result, a key challenge is to find methods to store energy from renewable and intermittent sources so that the stored energy is readily available [2-4]. The storage of renewable energy in the form of energy-rich molecules (hydrogen, ammonia, and methanol) has been proposed as a solution [2, 3, 5]. Currently, most hydrogen is produced through steam reforming, a process that depends on fossil fuels and has a large carbon footprint [6, 7]. Water electrolysis is an alternative process to produce hydrogen [7]. Electrolyzers are suited to be directly coupled with electric power generated from renewable energy sources, where hydrogen and oxygen are produced from water [2]. Alkaline electrolysis (AEL) is one of the large scale alternatives for the electrochemical production of hydrogen [4]. Currently, one of the main hurdles is the energy consumption, which depends on the cell voltage needed for water splitting [8, 9]. Technological efforts have been focused on the development of electrocatalysts to reduce the required cell voltage, thus lowering the cost. Platinum (Pt) is considered one of the best hydrogen evolution reaction (HER) catalysts under acidic conditions, with extremely low overpotentials and large currents [9, 10]. However, Pt faces limitations for scale-up applications due to the high cost and scarcity of noble metals. Earthabundant transition metals are a lower-cost alternative that could enable large-scale production and

implementation of alkaline electrolyzers if high activity and durability can be achieved, as compared to Pt as the benchmark comparison for both acidic and alkaline systems.

44

45

46

47

48

49

50

51

52

53

54

55

56

57

58

59

60

61

62

Nickel (Ni) is a well-known HER catalyst for water electrolysis in alkaline media [9, 10]. Efforts have been made to increase the activity and stability of Ni-based catalysts through different approaches, including increased active surface area and the development of Ni-based alloys. HER current density can be increased as the electrochemical surface area (ECSA) is increased for Nibased electrodeposited catalysts [11]. However, the activity is limited by the intrinsic activity of the catalyst composition [10]. The intrinsic activity is most accurately described by the turnover frequency (TOF). However, due to the difficulty of determining the TOF, in electrocatalysis it has been commonly adopted to use the specific activity to represent the intrinsic activity. Therefore, the intrinsic activity is most commonly defined as the specific activity where the current is normalized by the real surface area of the electrocatalyst. The incorporation of additional components to form Ni-based alloys such as molybdenum (Mo) [12], cobalt (Co) [13], and iron (Fe) [14] have shown to influence HER activity positively by increasing either the intrinsic catalytic activity or the long term stability. Through the combination of different elements, the intrinsic activity of a catalyst can be improved through a synergistic effect among the components. Alloys can change the electronic structure of the catalyst, and chemical environment changes can positively influence HER activity through effects on charge transport, charge redistribution, and reduction of energy barriers [10, 15-17]. However, it has also been shown that incorporation of other components can change the catalyst surface area [12, 18, 19]. Thus, when different catalysts are compared, it is crucial to delineate the cause for such observed changes in HER performance.

Since both the active surface area and the intrinsic electroactivity can affect measured activity, it is important to experimentally determine the active surface area of the electrocatalyst. Such an evaluation and distinction has demonstrated that Ni-Co and Ni₃S₂@Co(OH)₂ compositions result in an increase in intrinsic HER activity through synergistic effects among the components [15, 20]. On the other hand, a study of the surface composition, crystallite size, and surface area of a Febased catalyst allowed Muller et al. [19] to demonstrate that the incorporation of the metalloids silicon (Si) and boron (B) caused an increase in HER activity due to an increase in surface area, but the integration of Co increased the intrinsic HER activity. With Ni, Fe has been demonstrated to prevent nickel hydride phase formation, which prevents deactivation and improves the stability of Ni catalysts [21]. Therefore, Fe has been frequently implemented in Ni-based catalysts with compositions such as NiFeS/NF [14], Pt-FeNi@C [22], FeNi-P/NF [23], and NiFe/NC [24] due to the stability it provides. Nonetheless, the benefits of Fe as a transition metal dopant for Ni-based electrocatalysts for HER are not clear because active surface area and intrinsic activity have not been fully and separately evaluated. Navarro-Flores et al. [25] concluded that the overall electrocatalytic activity of bi-metallic Fe-Ni films for acidic HER was greater than that of pure Ni due to changes in surface roughness but the authors point out that the intrinsic electrocatalytic activity of bi-metallic Ni-Fe was actually lower than that of pure Ni films. However, at the same time, Navarro-Flores et al. [25] suggest that differences between Ni and Ni-Fe activity could be due to an oxide film on the catalyst surface. However, the authors do not provide a chemical analysis of the catalyst surfaces to clearly show these differences. In alkaline media, Solmaz et al. [26] concluded that Fe-Ni alloy films increased HER performance compared to mono-metallic Fe and Ni films. In addition, Solmaz et al. [26]

63

64

65

66

67

68

69

70

71

72

73

74

75

76

77

78

79

80

81

82

83

proposed that a film synthesized from a 4:6 molar concentration ratio of Ni²⁺:Fe²⁺ precursors was the best cathode for HER. Surface area variability between films was observed from atomic force microscopy (AFM) and EIS measurements, but a full evaluation of the intrinsic activity taking in consideration the differences in surface area was not performed; experimentally-determined bimetallic ratio was not reported. Nonetheless, the study by Solmaz et al. [26] is of importance as it focused on testing the catalysts for extended periods (24 and 120 h) and evaluated the catalysts based on corrosion and long-term stability, further demonstrating that incorporation of Fe increases the stability of Ni-based catalysts during HER. Using the electrodeposition synthesis method developed by Solmaz et al., [26] McCrory et al. [27] benchmarked Fe, Ni, and FeNi electrocatalyst films in acid and base. When electrocatalyst films were compared at 10 mA cm⁻² (geometric surface area), NiFe films outperformed both monometallic Fe and Ni in alkaline HER activity. McCrory et al. [27] reported that the roughness factor of the films increased in the order of Ni < Fe < NiFe, suggesting that surface roughness differences were the source of FeNi HER activity enhancement. This result indirectly demonstrates that the intrinsic activity of Ni may in fact be higher than that of Fe and NiFe films. However, the authors did not determine the experimental bi-metallic composition of the films, nor was an analysis of element-specific speciation and surface chemistry performed, leaving questions around the roles of composition and chemical structure. An evaluation of the physical surface area of Fe-Ni films was performed by Hu et al. [18]. A profilometer was used to determine the mean roughness factor and demonstrate that the surface roughness depends on the Fe-Ni film composition. Hu et al. [18] suggested that the HER of Fe-Ni films mainly depended on the true physical surface area. However, the study did not determine the electrochemically active surface area.

85

86

87

88

89

90

91

92

93

94

95

96

97

98

99

100

101

102

103

104

105

In contrast to these studies, a study performed by Suffredini et al. [28] is, to the best of our knowledge, the only study to attribute the increase in HER activity of Ni-Fe alloy films to an intrinsic synergistic effect. A clear explanation as to how such a synergistic effect could happen is not provided, but Suffredini et al. [28] point out that such observation is only possible on rough surfaces as the area enhancement is minimal. Conflicting evidence was recently reported by Zhang et al. [24] on nanoparticles, demonstrating that HER activity decreases with an increase in Fe content, but a Ni0.9Feo.1/NC was ultimately selected in the study as it showed excellent stability for HER and the best performance as a bifunctional OER and HER catalyst. There thus remains a gap in the field in terms of understanding the role of Fe in Ni electrocatalyst activity for the HER, and there is a lack of a complete study focused on elucidating the effect of Fe composition on HER in Fe-Ni films. Studies do consistently show increased Ni durability when Fe is included in the catalyst composition, motivating further delineation of the role of Fe on activity.

To understand whether an Fe dopant into Ni electrocatalysts does in fact enhance the HER and to understand the chemical nature of the electrocatalyst surface, we thus pursued a study on a suite of electrodeposited Fe_xNi_{100-x} films. We focus herein on understanding whether surface area or intrinsic activity is the main effect responsible for HER activity on different Ni-Fe bi-metallic catalysts in alkaline media. In addition, we probe the surface chemistry of this electrocatalyst suite to understand metallic and oxide contributions to the as-synthesized films. Film morphology was studied by scanning electron microscopy (SEM), and the composition of as-deposited samples was determined by energy dispersive x-ray spectroscopy (EDX), x-ray photoelectron spectroscopy (XPS), and inductive coupled plasma mass spectrometry (ICP-MS). The electronic structure was evaluated through XPS and EIS.

Surface chemistry analysis suggests as-synthesized films are composed of a metallic subsurface with a top oxidic layer. However, when films were tested in alkaline electrolyte, cyclic voltammetry analysis demonstrated that Ni on the surface is fully reduced, but Fe can be found as Fe²⁺ and Fe⁰. The ECSA was determined and used to compare the intrinsic electrochemical activity of the different catalysts. We have found that the electrochemically active surface area depends on the composition and in general increases with the incorporation of Fe. The bi-metallic film with the lowest overpotential needed to reach -10 mA cm⁻² was Fe₅₀Ni₅₀ demonstrating to have the highest geometric surface area normalized HER activity, which we attribute to the high ECSA. We thus demonstrate in this study that the HER activities observed for electrodeposited Fe_xNi₁₀₀-x films are likely due to changes in surface area, which depend on the composition, rather than by an enhancement of the intrinsic catalytic activity of the components.

2. Experimental Section

2.1. Materials

The following chemicals were purchased and used without further purification. Iron(II) sulfate heptahydrate (FeSO₄·7H₂O) (\geq 99.0% Sigma-Aldrich), nickel(II) sulfate hexahydrate (NiSO₄·6H₂O) (\geq 99.99% Sigma-Aldrich), boric acid (H₃BO₃) (\geq 99.5% Sigma-Aldrich), 70% nitric acid (HNO₃) (\geq 99.999% Sigma-Aldrich), concentrated sulfuric acid (H₂SO₄) (ACS reagent Sigma-Aldrich), and iron and nickel ICP standards (Aristar, BDH). Ultrapure water (18.2 M Ω ·cm) was obtained from a Milli-Q system. Gold coated silicon wafers (100 nm gold, 5 nm titanium) were purchased from Platypus Technologies and Au with Ti adhesion 5 MHz quartz crystals from Biolin Scientific.

2.2. Synthesis of Fe_xNi_{100-x} Heterogeneous Catalysts

Different Fe_xNi_{100-x} ratios were directly deposited on conductive substrates using cathodic electrodeposition. The substrate used were silicon wafers coated with 100 nm gold. Wafers were cut into 1 cm x 2 cm rectangles and later covered with Kapton tape in order to limit the area exposed to the electrolyte to about 1 cm². A three-electrode electrochemical system was used to hold the potentials at (-1.5V) for 30 seconds, where Ag/AgCl (3M NaCl) was used as the reference electrode, and a graphite rod was used as the counter electrode.

Solution of different ratios (Table S1) of Fe_xNi_{100-x} salts were prepared to produce the desired compositions of Fe_xNi_{100-x} catalyst films from a 150 ml plating bath. For each synthesized film, an aqueous solution of 0.1 M total metal content of iron(II) sulfate heptahydrate and nickel(II) sulfate hexahydrate, and 0.1 M of boric acid, was prepared accordingly. The ultrapure water (18.2 M Ω ·cm resistance) used to prepare the deposition bath was deaerated for 30 min with Argon before being used and also while the solution was being mixed to dissolve the salts and prevent Fe oxidation and precipitation. Afterward, the deposited films were rinsed with water (18.2 M Ω ·cm resistance) and dried with nitrogen gas to remove any excess deposition bath solution. To prevent contamination between different syntheses, all materials used during the deposition were soaked in 1 M sulfuric acid and rinsed thoroughly with water (18.2 M Ω ·cm resistance) to clean surfaces and prior to the next synthesis.

2.3. Physical Characterization

Quartz crystal microbalance with dissipation monitoring (QCM-D) from Biolin Scientific was used to determine mass loaded after film synthesis. The change in mass per unit area (Δm) was

calculated using the Sauerbrey equation ($\Delta f = -C_f \times \Delta m$), where (C_f) is the sensitivity factor of the AT-cut quartz-crystal sensor and (Δf) is the measured frequency change [29].

Scanning electron microscopy (SEM) (Nova Nanolab 200 5 keV) was implemented to study the surface morphology, and electron dispersive X-ray spectroscopy (EDX) was used to find the relative atomic ratio of Fe and Ni in the films. X-ray photoelectron spectroscopy (XPS) was carried out on a VersaProbe 5000 station from Physical Electronics with a monochromated Al Kα X-ray source. All XPS data analysis was performed with the PHI MultiPack software. The survey scans were used to find the Fe_xNi_{100-x} ratio of the electrocatalyst surface. Additionally, C 1s, O 1s, Fe 2p, and Ni 2p detailed regions were scanned to further study the surface chemistry. Inductive coupled plasma mass spectrometry (ICP-MS) was performed using IcapQ ICP-MS (Thermo Scientific) to quantify and confirm the bulk Fe and Ni composition of the electrodeposited catalysts. Films were digested in concentrated nitric acid and later diluted to a final 2% nitric acid. A matrix of 2% nitric acid was used to dilute the ICP standards and as a blank.

2.4. Electrochemical Characterization

All electrochemical experiments were performed with a VSP-300 BioLogic potentiostat using an H-cell separated by a Celgard 3401 (25 μM thickness) membrane with a three-electrode system. A graphite rod was used as the counter electrode, Ag/AgCl (3 M NaCl) as the reference electrode, and different Fe_xNi_{100-x} ratios as working electrodes. For all experiments, the electrolyte was deaerated with argon for 30 min before the tests, and Ar was used to purge the headspace during the electrochemical analysis.

The uncompensated resistance between the reference electrode and the working electrode was corrected by compensating at 85% IR drop, using the BioLogic EC-Lab software. The uncompensated resistance was measured by performing an impedance measurement at high frequencies (100 kHz) with a 20 mV sinusoidal amplitude at open-circuit potential (OCP). All electrochemical experiments were performed in 1 M NaOH at pH 12.00, with pH controlled through the addition of sulfuric acid. CVs were performed for ten cycles in the potential range (0.2 V to -0.5 V vs. RHE) at a 50 mV s⁻¹ scan rate to evaluate their catalytic characteristics under alkaline media (Fig. S3). Furthermore, linear sweep voltammetry (LSV) was performed at a scan rate of 5 mV s⁻¹ in the same potential window used for the CV.

The ECSA was estimated through the cyclic voltammetry method; a method used to benchmark numerous electrocatalysts for HER [27]. Under a non-Faradaic region, a series of CV scans were performed at different scan rates (25, 50, 100, 200 mV s⁻¹). The average difference between the anodic and cathodic charging current densities were plotted as a function of scan rate, Fig. 3S(a-e). The double-layer capacitance (C_{dl}) was found by obtaining the slope of the linear fit. The ECSA of each different Fe_xNi_{100-x} catalyst was estimated by dividing the C_{dl} found by the specific capacitance. The specific capacitance used for our calculations was (0.040 mF cm⁻²), commonly used for metals in 1 M NaOH [27, 30].

3. Results and Discussion

3.1. Composition and Morphology

Prior to electrochemical analysis of the synthesized Fe_xNi_{100-x} films, several complementary characterization techniques were used to confirm both the bulk and the surface composition of the

films. In particular, characterization of the films was pursued to determine if the composition of the samples deposited was consistent and reproducible and if the theoretical and experimental compositions were the same. Surface/near-surface elemental quantification of Fe and Ni content was initially determined by EDX and XPS. PHI MultiPack software was used for the quantification analysis of the XPS survey spectra. Fe and Ni relative content were obtained by using the Fe 3s and Ni 3s binding energy regions (Fig. S2) of XPS data to avoid any issues in analysis resulting from the overlap of the Fe 2p binding region and the Ni LMM Auger region. The influence of the Ni LMM Auger peaks on the Fe 2p region can be observed in the spectrum for Fe₀Ni₁₀₀ in Fig. 1b (purple spectrum), where based on calculations using the Fe 3s peak, no Fe was detected. The results in Fig. 1a demonstrate that the surface composition was tuned according to the theoretical ratios of the deposition bath with minimal variation between replicates (n=3). The compositions determined by XPS and EDX are quite similar, and no major deviations or differences are observed across the compositional space explored. Additionally, the bulk composition of the electrodeposited films was determined by ICP-MS. As demonstrated in Fig. 1a, the bulk composition of each film matches the surface composition determined through EDX and XPS. The bulk ICP measurements (Fig. 1a) further confirm that each film was deposited according to the theoretical composition. These results demonstrate that the synthesis method allows compositional tunability and reproducibility of electrocatalyst films with the desired composition. Additionally, electrodeposition of the different Fe_xNi_{100-x} films was performed on a gold (Au) sensor with a titanium adhesion layer (Ti) (5 MHz quartz crystal with Au-Ti coating layers) and analyzed with a quartz crystal microbalance with dissipation monitoring (QCM-D). Through the QCM-D analysis of replicated (n=3) depositions (Table S2), we demonstrate that our synthesis technique

212

213

214

215

216

217

218

219

220

221

222

223

224

225

226

227

228

229

230

231

232

allows for consistent and repeatable mass deposition. Most compositions deposit a film of around $60~\mu g~cm^{-2}$ except for the Fe₈₀Ni₂₀ ratio, which was around half that value, or $\sim 30~\mu g~cm^{-2}$ (Table S2).

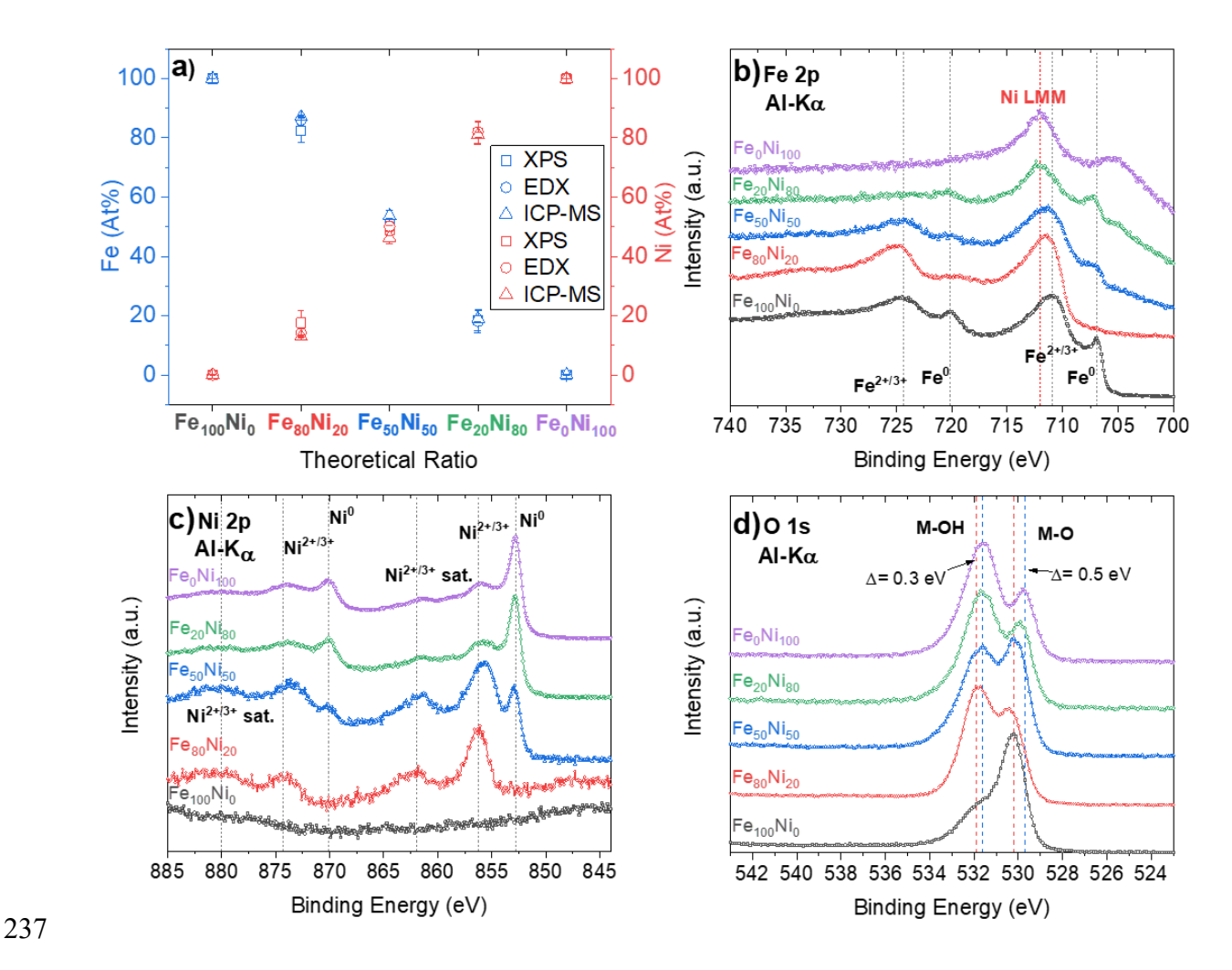


Fig. 1. a) Atomic percent of Fe and Ni electrodeposited of as-synthesized films. XPS spectra of b) Fe 2p c) Ni 2p and d) O 1s of the as-synthesized films.

The morphology of the as-deposited samples was also examined. SEM images were obtained of the top surfaces of all the synthesized Fe_xNi_{100-x} films. The images for the different samples (Fig.

S1) demonstrate that the morphology of the electrodeposited surface varies depending on the Fe_xNi_{100-x} composition. The electrodeposited surfaces of Ni-rich films appear to be more homogeneous and smooth, with less visible clusters, compared to those where Fe is present in higher amounts. The largest clusters with a spherical shape and a diameter of around 2 μm were observed on Fe₈₀Ni₂₀. The clusters decrease in size to a sub-micron scale on Fe₅₀Ni₅₀ samples and then become un-detectable for Fe₂₀Ni₈₀ and Fe₀Ni₁₀₀. The images obtained suggest there is likely to be a difference in surface area due to the topological variation among samples of different compositions. However, an ECSA analysis is ultimately necessarily to evaluate the active and electrochemically-accessible surface area of the films.

3.2. Analysis of Film Surface Chemistry

The XPS survey spectra (Fig. S2) revealed the presence of Fe, Ni, oxygen (O), and carbon (C) on the surface of the as-deposited samples. High-resolution XPS scans were performed on the Fe 2p, Ni 2p, and O 1s binding energy regions (Fig. 1b-d) to investigate the chemical state of these elements in the surfaces of the different as-deposited Fe_xNi_{100-x} films. All XPS spectra were calibrated by the C 1s peak (284.8 eV). Fe 2p spectra (Fig. 1b) reveal peaks at binding energies of 706.9 eV and 720.2 eV, which can be assigned to the Fe 2p_{3/2} and Fe 2p_{1/2} of metallic Fe⁰ [31-33]. In addition, peaks around 711 eV and 724 eV correspond to the Fe 2p_{3/2} and Fe 2p_{1/2} of oxidic iron [31-33]. Iron phases with a higher oxidation state (Fe₃O₄, Fe₂O₃, and FeOOH) have similar XPS spectra (shape and peak positioning) [33]. Recognizing the difficulty in distinguishing between Fe speciation, to avoid reporting misleading interpretations, and in agreement to other studies [34, 35], we acknowledge the possibility of having Fe²⁺ and Fe³⁺ but due to the strong overlap in peak location, we group them as oxidic iron. Our results agree with those results obtained on deposited

Fe films by Louie et al., [35] where peaks at 707 eV and 720 eV were assigned to metallic iron and the main oxidic peak was identified at 710.8 eV. There are no apparent metallic iron features in the spectra of as-deposited Fe₈₀Ni₂₀ samples; however, after the sample was argon-ion sputter cleaned, metallic Fe features were revealed (Fig. S3), suggesting that the Fe₈₀Ni₂₀ film had a thicker surface oxidic layer. Hu et al. [34] compared an Fe foil after it was oxidized and later electrochemically reduced, with XPS results similar to our results. The Fe 2p spectra and peak positions of our as-deposited Fe₈₀Ni₂₀ film match that of the fully oxidized iron foil with a main peak at 711 eV assigned to the oxidic iron species. In addition, the metallic peak around 707 eV was also observed by Hu et al. [34] post reduction of the iron foil. Overall, these results confirmed the presence of oxidic and metallic iron.

The Ni 2p spectra (Fig. 1c) reveal that samples electrodeposited contain metallic and oxidic components. The peaks at around 852.8 eV and 870.1 eV correspond to the Ni 2p_{3/2} and Ni 2p_{1/2} of metallic (Ni⁰) nickel, respectively [31, 36-38]. Peaks at 856.2 eV and 874.3 eV correspond to Ni 2p_{3/2} and Ni 2p_{1/2} of the oxidic nickel with their respective satellites at 861.9 eV and 880 eV (broad peaks) [36-38]. The Fe₁₀₀Ni₀ spectrum demonstrates the absence of Ni in samples electrodeposited (Fig. 1c). Ratios Fe₀Ni₁₀₀, Fe₂₀Ni₈₀, and Fe₅₀Ni₅₀ contain both metallic and oxidic nickel as-deposited. As observed in the Fe 2p spectra, the as-deposited Fe₈₀Ni₂₀ sample is the only sample that shows no significant metallic nickel components. The Ni 2p spectra of Fe₈₀Ni₂₀ closely resembles that of Ni films deposited and studied by Louie et al. [35] in analyses performed on as-deposited films and post oxidation. We suggest that the oxidic nickel could be Ni(OH)₂ and a type of NiOOH, and suspect none or small amounts of NiO due to the absence of the splitting of the Ni 2p_{3/2}. However, additional work, as done by Biesinger et al., [37, 38] would be required to identify

the oxidic nickel through the implementation of an analysis of the Ni LMM Auger spectra. After argon ion sputter cleaning, metallic nickel features for all compositions become noticeable (Fig. S3). The Ni 2p spectra post argon ion sputtering resemble those of NiFe nanocarbon hydrides that were fully reduced through pyrolysis [24]. These results confirm the oxidation of the surface but demonstrate that a metallic Ni sub-surface was deposited. Overall, these results confirmed the presence of oxidic and metallic nickel. The O 1s spectra (Fig. 1d) for the different Fe_xNi_{100-x} compounds show the presence of two species. The peak at a lower binding energy of 530.2 eV corresponds to metal-oxygen species (i.e., M-O), while the peak at 531.6 eV is assigned to metal hydroxide species (i.e., M-OH) [32]. The ratio of M-O and M-OH is different depending on the composition, as observed in Fig. 1d. Fe₀Ni₁₀₀ has higher M-OH content, and Fe₁₀₀Ni₀ has higher M-O content. As shown by Shi et al., [39] the oxidation kinetics for Fe-Ni alloys depends on the composition. From the O 1s spectra, we can note that M-OH and M-O shift 0.3 eV and 0.5 eV, respectively. O 1s peaks for Fe₀Ni₁₀₀ are found at lower binding energies, and peaks for Fe₁₀₀Ni₀ are found at higher binding energies, correlating to what has been published in literature for different Fe and Ni standards [32]. After argon ion sputtering, a reduction of the M-OH on all samples was observed, suggesting that M-OH is found on the uppermost layer. Such results agree with studies on the oxidation of Fe-Ni alloys, which showed that different layers of oxides can be formed [39]. These results provide insight as to what the surface oxidation most likely resembles after the outer most surface is reduced. In support of the Fe and Ni results, the O 1s spectra demonstrate the presence of multiple oxidic metal components. The inherent oxidation of the samples is expected due to the use of an aqueous bath

during synthesis and the consequent exposure of the samples to atmospheric conditions.

286

287

288

289

290

291

292

293

294

295

296

297

298

299

300

301

302

303

304

305

306

As mentioned, different Ni and Fe components are found on the surface of the films. Bi-metallic M-OH and M-O change with composition but are found to contribute to the surface chemistry of both pure metal films. Such differences can be attributed to the mixed surface species formed depending on the presence of Fe or Ni at the surface. The O 1s spectra demonstrate how, based on the composition of the surface, the metal-oxygen speciation is altered. A significant difference in the Fe 2p and Ni 2p peak positions is not apparent throughout our Fe_xNi_{100-x} films, but the change in metallic and oxidic components with composition could suggest bi-metallic interactions. Similar to our study, Hong et al. [40] studied Ni and Co films that were simultaneously electrochemically deposited. A shift in peak positions of the Ni 2p was minimal; however, Hong et al. [40] also observed a difference in the proportion of the oxidic and metallic species based on the composition. Such differences led Hong et al. [40] to suggest an electronic interaction between the Ni and Co components. Therefore, we attribute the difference in proportions of oxidic and metallic species though out the Fe_xNi_{100-x} films to be due electronic interactions between the Fe and Ni components.

3.3. Hydrogen Evolution Reaction Performance

The HER activity for the different as-deposited Fe_xNi_{100-x} ratios and control samples (Au, Pt) were examined under alkaline conditions using an H-cell three-electrode system. All surfaces were initially cycled in the alkaline electrolyte for ten cycles to stabilize the surfaces and obtain consistent cyclic voltammograms (CVs), Fig. S4c. The CVs were performed from 0.2 V vs RHE to -0.5 V vs RHE. The initial cycle deviates from the subsequent cycles, which can be attributed to the reduction of the different oxidic species present on the surface, Fig. S4a. The stabilized CVs of the Fe containing surfaces closely resemble those previously reported for Fe in alkaline solutions [26, 41, 42]. Within the potential window of interest, Fe goes through a quasi-reversible

reduction oxidation process involving Fe⁰ and Fe²⁺. The cathodic peak of the stabilized CV appears to have two components, Fig. S4. It has been demonstrated that the reduction of iron oxides/oxyhydroxides and Fe²⁺ in alkaline solutions on an iron sheet and sputtered film happen at close potentials [41]. Thus, the smaller shoulder of the cathodic peak can be attributed to the reduction of Fe oxides/hydroxides that have not been reduced in previous cycles. On the other hand, nickel is fully reduced after the first cycle, Fig. S4b. It has been previously shown that Ni will oxidize at higher potentials in alkaline conditions [26, 43-45] not reached in our experiments. Thus, we conclude that nickel in the deposited films under the conditions of interest are found as Ni⁰. As previously mentioned, the main purpose of performing the CVs was to stabilize the surface. Nonetheless, these results help to support the analysis previously reported on the surface chemistry. The results of Fig. 2a show a comparison of the linear sweep voltammograms (LSV), where the IR-corrected voltage in the RHE scale is plotted against the geometric surface area normalized current; the inset of Fig. 2a shows a comparison of the measured overpotentials taken at -10 mA cm⁻². In order to ensure that the LSV was performed in a kinetically limited region, the LSV was performed at different stir rates, Fig S6. The LSV results overlap at different stirring rates showing the lack of mass transport limitations and confirming that the data were obtained in a kinetically limited region. The geometric surface area used for the normalization of the current was 1 cm² for the different Fe_xNi_{100-x} synthesized samples and Au and 0.159 cm² for the Pt wire. When evaluating the geometric area normalized HER activity (i.e., current density measured at -0.5 V vs. RHE), the synthesized materials followed the order: $Fe_{80}Ni_{20} \approx Fe_{0}Ni_{100} \approx Fe_{50}Ni_{50} > Fe_{100}Ni_{0} > Fe_{20}Ni_{80}$ (Table S6). A widely used parameter to compare different catalysts is the determined overpotential

330

331

332

333

334

335

336

337

338

339

340

341

342

343

344

345

346

347

348

349

350

needed to reach a current density of -10 mA cm⁻². The inset graph in Fig. 2a shows that the overpotential needed to reach a current density of -10 mA cm⁻² does not follow a trend with respect to Fe_xNi_{100-x} composition. However, Fe₅₀Ni₅₀ has the lowest overpotential (-390 mV), while Fe₁₀₀Ni₀ has the largest overpotential (-443 mV) needed to drive a current density of -10 mA cm⁻².

Solmaz and Kardas studied Fe-Ni electrodeposited films and concluded that bi-metallic films were more active electrocatalytically when compared to mono-metallic films and further identified a specific composition as the optimal cathode for HER [26]. The highest HER electroactivity was obtained on films from a precursor aqueous plating bath with a concentration ratio of 4Ni²⁺:6Fe²⁺, when evaluated in 1M KOH at room temperature [26]. In a later study, Fe-Ni alloy films were evaluated in 25 wt% KOH at 80 °C [46]. Flis-Kabulska and Flis determined that the HER activity increased with increase of Fe content up to 90 wt% Fe, where the highest activity was reached [46]. Such studies agree to an extent with our results as we found that in our case a bi-metallic film of Fe₅₀Ni₅₀ composition was found to have the best HER performance (i.e., as measured by both current density and overpotential) when normalized by geometric surface area. However, we observe that bi-metallic surfaces do not outperform monometallic surfaces in all cases.

and Flis focused on evaluating different Fe-Ni compositions for their extended HER activity to determine Fe-Ni sample stability. However, these studies lack an evaluation of active surface area. As noted previously in our SEM results, there is a morphological difference that occurs as the composition changes. Such a morphological difference is also evident in the SEM and AFM results presented in the study of the Fe-Ni films by Solmaz and Kardas [26]. However, the authors do not

It is important to highlight that the studies performed by Solmaz and Kardas and by Flis-Kabulska

discuss this aspect in detail and the role of the surface morphology is left out of the evaluation of catalyst activity. To address this gap and further our understanding of these details, additional electrochemical analyses were performed to understand the effect of these morphology changes as the Fe-Ni catalyst composition changes and the overall impact on HER activity.

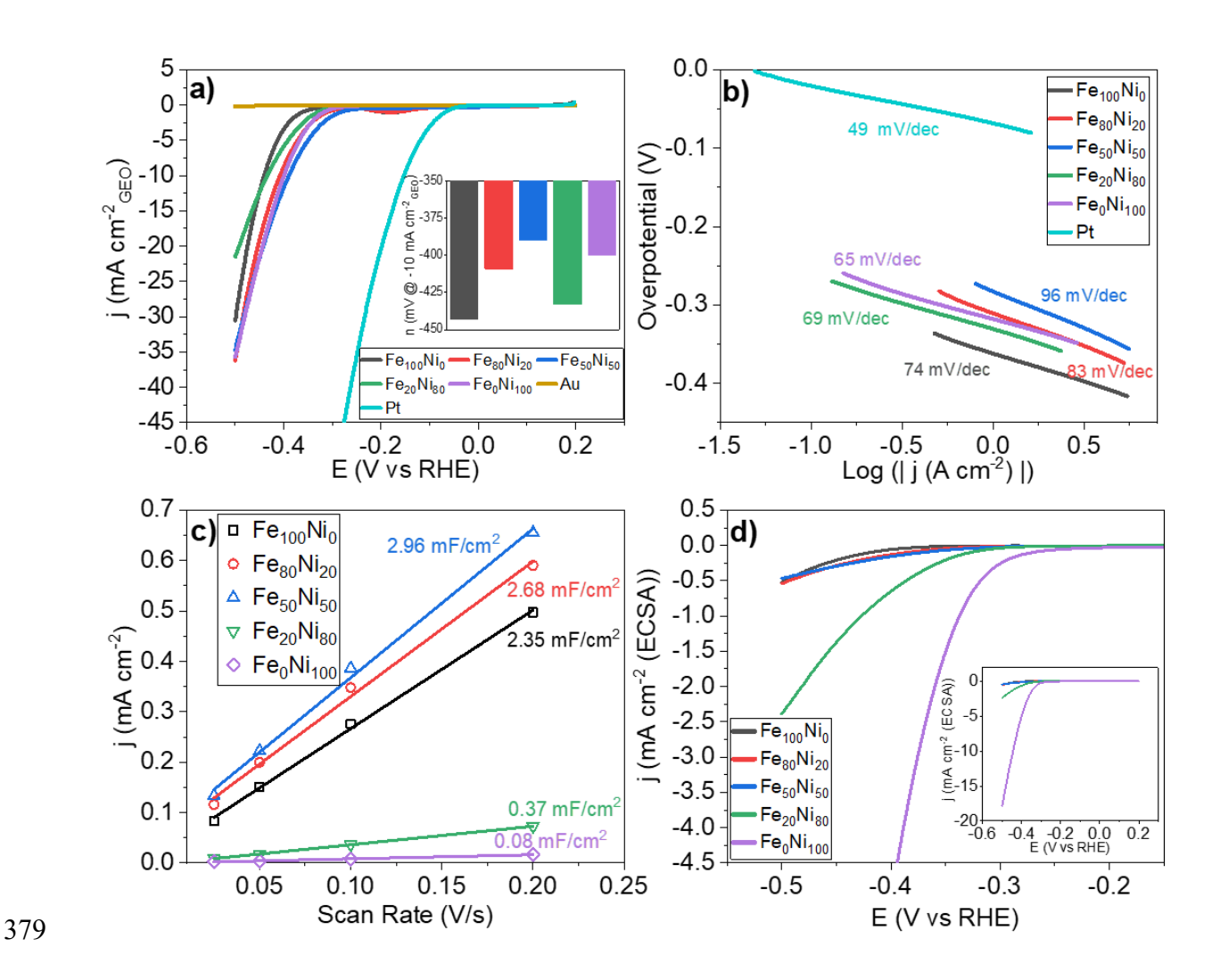


Fig. 2. a) LSV of different Fe_xNi_{100-x}, Au, and Pt in 1M NaOH (pH=12) normalized by geometric surface area. b) Tafel plots of Fe_xNi_{100-x} and Pt. c) calculated double-layer capacitance (C_{dl}) used to estimate the electrochemically active surface area of the different Fe_xNi_{100-x} samples. d) LSV of different Fe_xNi_{100-x} normalized the estimated ECSA in 1M NaOH (pH=12).

First, based on the polarization curves from Fig. 2a, the Tafel plots of the different catalysts were determined to evaluate the reaction kinetics, Fig. 2b. Pt shows the lowest Tafel slope (49 mV dec

1), a value that correlates with those previously reported for Pt/C in 1 M NaOH (40 mV dec⁻¹) [13]. Generally, through our literature search, the HER Tafel slopes of different Fe and Ni based transition metal catalysts in alkaline electrolyte are found in the 60-120 mV dec⁻¹ range [13, 14, 23, 24, 46, 47]. The experimentally-determined Tafel slope values of the different Fe_xNi_{100-x} samples are in the range of 65-96 mV dec⁻¹, in accordance with other results published. The slopes separate the samples into two groups. The first group includes Fe₁₀₀Ni₀, Fe₈₀Ni₂₀, and Fe₅₀Ni₅₀ with higher slopes, while the compositions of Fe₂₀Ni₈₀ and Fe₀Ni₁₀₀ have lower slopes. Our result reveals favorable HER kinetics for samples with higher Ni content as Fe₂₀Ni₈₀ and Fe₀Ni₁₀₀. The obtained Tafel slopes suggest that overall, the samples follow the Volmer-Heyrovsky mechanism for HER [48, 49]. Additionally, the Tafel slope values that we obtain suggest that the electrochemical hydrogen desorption step through the Heyrovsky reaction (H₂O + e⁻ + H*→ H₂ + HO⁻) [47], is likely the rate-determining step. To elucidate the effect of composition on HER without any contribution due to differences in surface area, the electrochemically active surface area was determined. The electrochemically active surface area was estimated from the double layer capacitance obtained through the CV method. As shown in Fig. S5(a-e), CVs of a 0.1 V window were performed within a non-Faradaic region at different scan rates. The charging current at the different scan rates was plotted (Fig. 2c) to obtain the double layer capacitance from the slope. From Fig. 2c, we can observe a difference in orders of magnitude in the double layer capacitance (Cdl) between the films depending on the composition. Once again, the different Fe_xNi_{100-x} catalysts are separated into two groups, where Fe₁₀₀Ni₀, Fe₈₀Ni₂₀, and Fe₅₀Ni₅₀ compositions have high C_{dl} values and Fe₂₀Ni₈₀ and Fe₀Ni₁₀₀ compositions have low C_{dl} values. The ECSA was estimated using the specific capacitance (0.04

387

388

389

390

391

392

393

394

395

396

397

398

399

400

401

402

403

404

405

406

407

mF cm⁻²) commonly used for 1 M NaOH [27, 30]. Nonetheless, as Wei et al. [50] states, there is a need for additional work in this area to determine the specific capacitance of different materials and the development of a database in order to improve the accuracy of ECSA determination. Results are summarized in Fig. 4a. The ECSA values estimated for Fe₁₀₀Ni₀, Fe₈₀Ni₂₀, and Fe₅₀Ni₅₀ are an order of magnitude higher than that of Fe₂₀Ni₈₀ and Fe₀Ni₁₀₀. In agreement with SEM imaging, the samples with higher Fe have a higher electroactive surface area and thus more exposed sites. As noted previously, the Tafel slopes and the C_{dl} suggest an effect due to composition. The same compositional effect is not observed on the polarization curves presented in Fig. 2a. The C_{dl} results illustrate that the geometric surface area normalization polarization curves can be misleading and, in this case, would most certainly lead to incorrect conclusions about Fe_xNi_{100-x} catalyst activity, as the difference in electrochemically active surface area could be contributing to HER activity. As the surface topology can influence catalyst performance, the LSV data were normalized by the ECSA to determine the intrinsic HER activity for each catalyst (Fig. 2d). Normalization of the current by the ECSA (Fig. 2d) caused the order in HER activity to change from what was observed when the current was normalized by the geometric surface area (Fig. 2a). When normalized by the ECSA, only the pure nickel sample reached a current density of -10 mA/cm² at an overpotential of -444 mV vs. RHE, as seen in the inset of Fig. 2d. Therefore, the ECSA normalized specific current density at (-0.5 V vs. RHE) as shown in Fig. 2d was used to compare the samples. The HER activity followed the order: $Fe_0Ni_{100} > Fe_{20}Ni_{80} > Fe_{80}Ni_{20} \approx Fe_{100}Ni_0 \approx Fe_{50}Ni_{50}$, Fig. 2d. As expected, pure nickel is more active than pure iron. Thus, our results show that the intrinsic HER activity of bi-metallic Fe-Ni is lower than pure Ni and comparable to pure Fe, and an increase in

409

410

411

412

413

414

415

416

417

418

419

420

421

422

423

424

425

426

427

428

429

the intrinsic HER activity is only observed when Ni is the predominant component. To the best of our knowledge, the work by Zhang et al. [24] is the only other work published that studied the effect of Fe-Ni catalyst composition in alkaline media in a similar manner. Zhang et al. [24] similarly demonstrated with nanoparticles that Fe doping negatively affected the HER activity of the Ni_{1-x}Fe_x/NC (nanocarbon), as the HER activity decreased with an increase in Fe content. Even though the physical morphology of the two catalyst suites is different since the catalysts were nanoparticulate and included nanocarbon, the findings of Zhang et al. [24] for nanoparticle catalysts agree with our results on films. When the electrochemical activity of FexNi_{100-x} electrocatalysts is normalized to consider differences in the electrochemically active surface area, which previous studies of Fe-Ni films in base have lacked, the intrinsic activity of Ni is higher than that of Fe and bi-metallic Fe_xNi_{100-x} catalysts. To further study the electrochemical area and the catalyst specific activity of the different Fe_xNi₁₀₀x, EIS was performed at -300 mV overpotential. The impedance spectra of all Fe_xNi_{100-x} samples are presented in a Nyquist plot, Fig. 3. The Nyquist plot reveals one semi-circle for all samples, indicating that the EIS spectra can be well-described by a one-time constant model such as the Randles circuit. Consequently, the impedance spectra indicate that the HER is primarily controlled by a charge transfer process, as previously reported for coatings and films in acid and alkaline media [25, 26]. To further investigate, the EIS data were modeled using the electrical equivalent circuit diagram shown in Fig. 3; a tabular listing of results is summarized in Table S7. The charge transfer resistance (RCT) can be evaluated visually by comparing the size of the semi-circles; however, modeling the data provides an accurate and quantitative method to compare such a

parameter, R_{CT} describes the rate-determining charge transfer step, and therefore, R_{CT} is inversely

431

432

433

434

435

436

437

438

439

440

441

442

443

444

445

446

447

448

449

450

451

proportional to the current density [19]. It is widely accepted that lower charge transfer resistance is indicative of more efficient electron transfer, thus leading to a higher HER electrocatalytic activity [13, 15, 19, 23, 24, 26]. Therefore, many studies compare the RCT to compare the activity of different catalysts. When comparing our results based on the RCT, we observe that the Fe₀Ni₁₀₀ film has the lowest charge transfer resistance, thus suggesting the highest electrocatalytic HER activity. Overall, the R_{CT} decreases as the Fe content decreases for the Fe_xNi_{100-x} films, except for Fe₂₀Ni₈₀. Additionally, the C_{dl} was obtained from the fit of the Nyquist plots and used to determine the ECSA-EIS. The ECSA calculated through EIS demonstrates that the electrochemically active surface area changes as the composition of the deposited sample varies, Fig. 4a. In general, the ECSA determined through EIS was lower than that estimated through the CV method. Such small variation can be attributed to the reduction of surface area from gas bubbles forming on the surface due to the potential at which the EIS measurements were performed [19]; an additional factor that may affect EIS vs CV results is the assumed specific capacitance used in ECSA calculations. These results collectively support our conclusion that the HER activity differences between samples are due to differences in electrochemically active surface area.

453

454

455

456

457

458

459

460

461

462

463

464

465

466

467

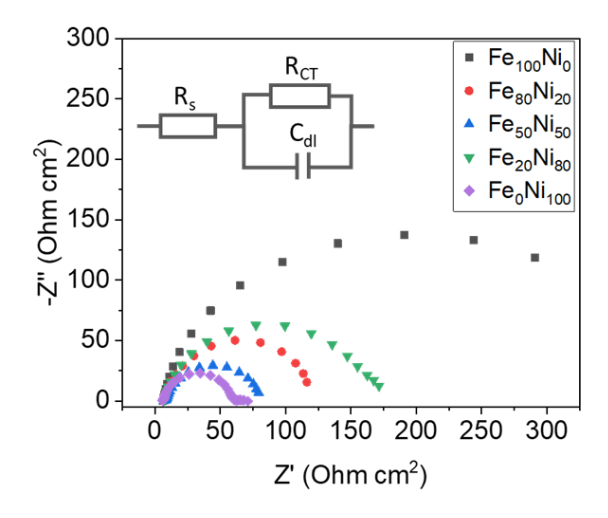


Fig. 3. Nyquist plot of EIS obtained at -300 mV in alkaline electrolyte.

The impedance results were further implemented to evaluate the catalytic activity in relation to the composition and active surface area of the different Fe_xNi_{100-x} films. The approach taken here quantitatively distinguishes the effect of composition from the effect of electrochemically active surface area on the HER activity. The intrinsic activity of each sample can be determined from the EIS data by τ , a parameter defined as $\tau = R_{CT} \ x \ C_{dl}$, representing the area-independent activity. Such a parameter has been implemented by Muller et al. [19] and allowed the authors to elucidate that the HER enhancement of Fe-based alloys when doped with metalloids (B and Si) is due to an increase in surface area whereas doping with Co results in an intrinsic effect. The τ parameter has also been used to study other transition metals such as Co and Co-vanadium (V) on Ni-based alloys [51] and molybdenum (Mo) on Ni-based alloys [52]. The parameter τ is inversely proportional to the specific activity since the charge transfer resistance (R_{CT}) is inversely proportional and the double-layer capacitance (C_{dl}) is directly proportional to the activity and active surface area, respectively [19]. All results are summarized in Table S7 and graphically illustrated in Fig. 4b. Since τ is inversely proportional to the specific activity, 1/ τ was plotted to compare the intrinsic

activity of each composition obtained through the EIS and ECSA normalized current density. The comparison of ECSA-normalized current and $1/\tau$ in Fig. 4b demonstrates that the specific activity of the samples increases as Ni content increases, thus supporting the results obtained from the current density normalized by ECSA rather than the current density normalized by geometric surface area.

The results presented throughout this study collectively indicate that the intrinsic catalytic activity in alkaline media of mono-metallic Ni films is greater than that of mono-metallic Fe or bi-metallic Fe_xNi_{100-x} films. In addition, when Fe is added to Ni films, the main factor influencing the HER activity is the increase of surface area. The major benefit of Fe doping in Ni-based catalysts remains the increase the long term stability [19, 21, 24, 46], and as shown herein, a possible method of enhancing the HER activity is through the increase of active surface area.

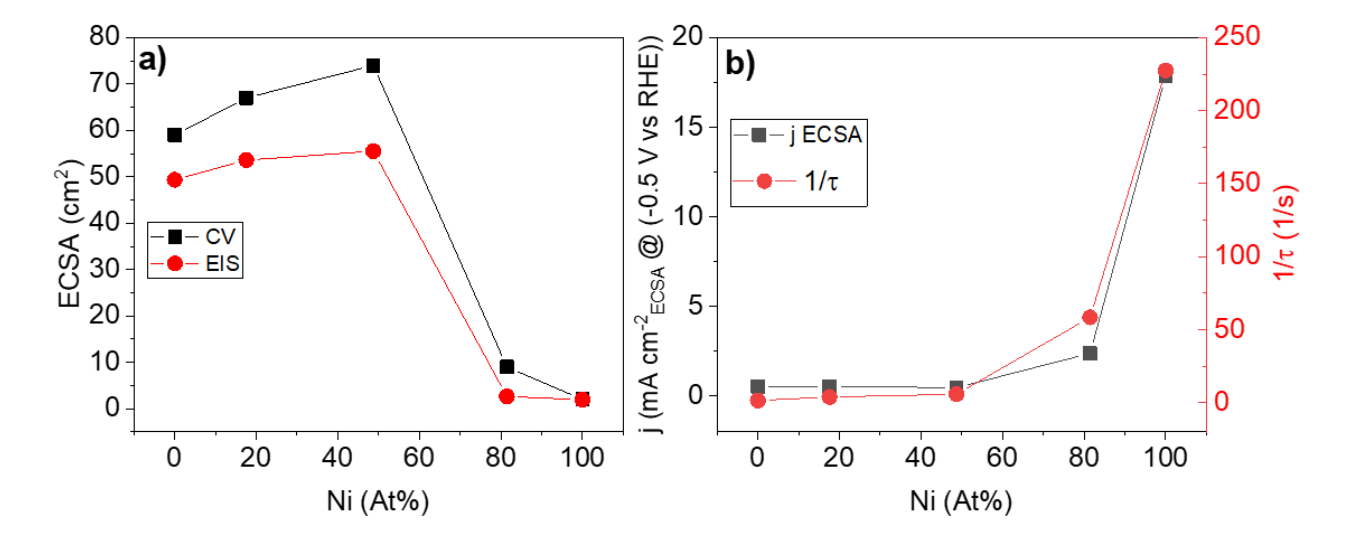


Fig. 4. a) Electrochemically active surface area for different Fe_xNi_{100-x} ratios obtained through the CV method and the EIS method. b) Specific current density and the specific activity $1/\tau$ parameter plotted for different compositions of Fe_xNi_{100-x} films, as determined through XPS.

4. Conclusions

500

501

502

503

504

505

506

507

508

509

510

511

512

513

514

515

516

517

In summary, Fe_xNi_{100-x} films have been synthesized through an electrodeposition method. The synthesis method was proven to provide composition tunability and reproducible synthesized films. The surface oxide and hydroxide species formed on the as-deposited surface are altered due to the composition. The HER electrochemical activity was studied based on the composition and electrochemically active surface area of the synthesized films. A bimetallic Fe₅₀Ni₅₀ film was found to be the most active as it required the lowest overpotential of -390 mV to reach a current density of -10 mA cm⁻² when normalized by geometric surface area. The ECSA was determined by the CV method and the EIS method, demonstrating that the ECSA was dependent on the sample composition and that in some cases, the difference in active surface area between films was above an order of magnitude. Intrinsic catalytic activity was obtained by normalizing each sample by the electrochemically active surface area and confirmed by obtaining an area-independent parameter, τ, through EIS. Such results demonstrated that mono-metallic Ni films have a greater intrinsic activity than that of mono-metallic Fe and even bi-metallic Fe_xNi_{100-x} films. We have found that the HER activity of Fe-Ni films is greatly influenced by the changes in active surface area, which are dependent on the composition. Thus, we conclude that the HER activity of different Fe_xNi₁₀₀x films in alkaline electrolyte can be attributed to the number of active sites rather than a synergistic effect of the components on intrinsic activity.

518

519

Declaration of Competing Interest

- 520 The authors declare that they have no know competing financial interests or personal relationships
- that could have appeared to influence the work reported in this paper.

522 Acknowledgments

- 523 S.I.P.B. and L.F.G. gratefully acknowledge support from the U.S. Department of Energy, Office
- of Science, Basic Energy Sciences, Catalysis Science Program, under award # DE-SC0016529.
- We thank Professor Clemens Heske and his group for the helpful discussions on XPS. We also
- 526 thank Professor Michael Janik for helpful electrochemistry and reaction mechanism discussions.

527 Appendix A. Supplementary material

- 528 Electrodepositing bath composition, QCM results, SEM images, XPS survey spectra and argon
- 529 sputtered spectra, CV results, LSV geometric and ECSA normalized data, and EIS results.

530 References

- 531 [1] C. Marcy, U.S. renewable electricity generation has doubled since 2008, in, U.S. Energy
- 532 Information Administration (EIA), 2019.
- 533 [2] N.S. Lewis, D.G. Nocera, Powering the planet: Chemical challenges in solar energy utilization,
- Proceedings of the National Academy of Sciences, 103 (2006) 15729-15735.
- 535 [3] H.B. Gray, Powering the planet with solar fuel, Nature chemistry, 1 (2009) 7-7.
- 536 [4] A. Buttler, H. Spliethoff, Current status of water electrolysis for energy storage, grid balancing
- and sector coupling via power-to-gas and power-to-liquids: A review, Renewable and Sustainable
- 538 Energy Reviews, 82 (2018) 2440-2454.

- 539 [5] G. Wang, A. Mitsos, W. Marquardt, Conceptual design of ammonia-based energy storage
- 540 system: System design and time-invariant performance, AIChE Journal, 63 (2017) 1620-1637.
- [6] G.W. Crabtree, M.S. Dresselhaus, M.V. Buchanan, The hydrogen economy, Physics today, 57
- 542 (2004) 39-44.
- [7] J.D. Holladay, J. Hu, D.L. King, Y. Wang, An overview of hydrogen production technologies,
- 544 Catalysis today, 139 (2009) 244-260.
- 545 [8] X. Li, X. Hao, A. Abudula, G. Guan, Nanostructured catalysts for electrochemical water
- splitting: current state and prospects, Journal of Materials Chemistry A, 4 (2016) 11973-12000.
- [9] K. Zeng, D. Zhang, Recent progress in alkaline water electrolysis for hydrogen production and
- applications, Progress in Energy and Combustion Science, 36 (2010) 307-326.
- 549 [10] M. Gong, D.-Y. Wang, C.-C. Chen, B.-J. Hwang, H. Dai, A mini review on nickel-based
- electrocatalysts for alkaline hydrogen evolution reaction, Nano Research, 9 (2016) 28-46.
- 551 [11] S.H. Ahn, S.J. Hwang, S.J. Yoo, I. Choi, H.-J. Kim, J.H. Jang, S.W. Nam, T.-H. Lim, T. Lim,
- 552 S.-K. Kim, Electrodeposited Ni dendrites with high activity and durability for hydrogen evolution
- reaction in alkaline water electrolysis, Journal of Materials Chemistry, 22 (2012) 15153-15159.
- 554 [12] P.M. Csernica, J.R. McKone, C.R. Mulzer, W.R. Dichtel, H.c.D. Abruña, F.J. DiSalvo,
- Electrochemical hydrogen evolution at ordered Mo7Ni7, ACS Catalysis, 7 (2017) 3375-3383.
- 556 [13] X. Yin, G. Sun, L. Wang, L. Bai, L. Su, Y. Wang, Q. Du, G. Shao, 3D hierarchical network
- NiCo2S4 nanoflakes grown on Ni foam as efficient bifunctional electrocatalysts for both hydrogen

- and oxygen evolution reaction in alkaline solution, International Journal of Hydrogen Energy, 42
- 559 (2017) 25267-25276.
- 560 [14] P. Ganesan, A. Sivanantham, S. Shanmugam, Inexpensive electrochemical synthesis of nickel
- 561 iron sulphides on nickel foam: super active and ultra-durable electrocatalysts for alkaline
- electrolyte membrane water electrolysis, Journal of Materials Chemistry A, 4 (2016) 16394-16402.
- 563 [15] S. Wang, L. Xu, W. Lu, Synergistic effect: hierarchical Ni3S2@ Co (OH) 2 heterostructure
- as efficient bifunctional electrocatalyst for overall water splitting, Applied Surface Science, 457
- 565 (2018) 156-163.
- 566 [16] Y. Yang, K. Zhang, H. Lin, X. Li, H.C. Chan, L. Yang, Q. Gao, MoS2–Ni3S2 heteronanorods
- as efficient and stable bifunctional electrocatalysts for overall water splitting, Acs Catalysis, 7
- 568 (2017) 2357-2366.
- 569 [17] Z. Xing, X. Yang, A.M. Asiri, X. Sun, Three-dimensional structures of MoS2@ Ni core/shell
- 570 nanosheets array toward synergetic electrocatalytic water splitting, ACS applied materials &
- 571 interfaces, 8 (2016) 14521-14526.
- 572 [18] C.-C. Hu, Y.-R. Wu, Bipolar performance of the electroplated iron–nickel deposits for water
- electrolysis, Materials chemistry and physics, 82 (2003) 588-596.
- 574 [19] C.I. Müller, K. Sellschopp, M. Tegel, T. Rauscher, B. Kieback, L. Röntzsch, The activity of
- 575 nanocrystalline Fe-based alloys as electrode materials for the hydrogen evolution reaction, Journal
- 576 of Power Sources, 304 (2016) 196-206.

- 577 [20] I. Herraiz-Cardona, E. Ortega, J.G. Antón, V. Pérez-Herranz, Assessment of the roughness
- 578 factor effect and the intrinsic catalytic activity for hydrogen evolution reaction on Ni-based
- electrodeposits, International journal of hydrogen energy, 36 (2011) 9428-9438.
- 580 [21] A.E. Mauer, D.W. Kirk, S.J. Thorpe, The role of iron in the prevention of nickel electrode
- deactivation in alkaline electrolysis, Electrochimica acta, 52 (2007) 3505-3509.
- 582 [22] A. Fan, C. Qin, X. Zhang, J. Yang, J. Ge, S. Wang, X. Yuan, S. Wang, X. Dai, Engineering
- 583 FeNi alloy nanoparticles via synergistic ultralow Pt doping and nanocarbon capsulation for
- efficient hydrogen evolution, Journal of Materials Chemistry A, 7 (2019) 24347-24355.
- 585 [23] Q. Yan, T. Wei, J. Wu, X. Yang, M. Zhu, K. Cheng, K. Ye, K. Zhu, J. Yan, D. Cao, Self-
- 586 supported FeNi-P nanosheets with thin amorphous layers for efficient electrocatalytic water
- 587 splitting, ACS Sustainable Chemistry & Engineering, 6 (2018) 9640-9648.
- 588 [24] X. Zhang, H. Xu, X. Li, Y. Li, T. Yang, Y. Liang, Facile synthesis of nickel–iron/nanocarbon
- 589 hybrids as advanced electrocatalysts for efficient water splitting, ACS Catalysis, 6 (2016) 580-
- 590 588.
- 591 [25] E. Navarro-Flores, Z. Chong, S. Omanovic, Characterization of Ni, NiMo, NiW and NiFe
- electroactive coatings as electrocatalysts for hydrogen evolution in an acidic medium, Journal of
- 593 Molecular Catalysis A: Chemical, 226 (2005) 179-197.
- 594 [26] R. Solmaz, G. Kardaş, Electrochemical deposition and characterization of NiFe coatings as
- 595 electrocatalytic materials for alkaline water electrolysis, Electrochimica Acta, 54 (2009) 3726-
- 596 3734.

- 597 [27] C.C.L. McCrory, S. Jung, I.M. Ferrer, S.M. Chatman, J.C. Peters, T.F. Jaramillo,
- 598 Benchmarking hydrogen evolving reaction and oxygen evolving reaction electrocatalysts for solar
- 599 water splitting devices, J. Am. Chem. Soc., 137 (2015) 4347-4357.
- 600 [28] H.B. Suffredini, J.L. Cerne, F.C. Crnkovic, S.A.S. Machado, L.A. Avaca, Recent
- developments in electrode materials for water electrolysis, International Journal of Hydrogen
- 602 Energy, 25 (2000) 415-423.
- 603 [29] G. Sauerbrey, Verwendung von schwingquarzen zur wägung dünner schichten und zur
- mikrowägung, Zeitschrift für Physik, 155 (1959) 206-222.
- 605 [30] C.C. McCrory, S. Jung, J.C. Peters, T.F. Jaramillo, Benchmarking heterogeneous
- electrocatalysts for the oxygen evolution reaction, Journal of the American Chemical Society, 135
- 607 (2013) 16977-16987.
- 608 [31] J.F. Moulder, W.F. Strickle, P.E. Sobol, K.D. Bomben, Handbook of X-ray photoelectron
- spectroscopy, Perkin-Elmer Corporation, 40 (1992) 221.
- 610 [32] M.C. Biesinger, B.P. Payne, A.P. Grosvenor, L.W.M. Lau, A.R. Gerson, R.S.C. Smart,
- Resolving surface chemical states in XPS analysis of first row transition metals, oxides and
- 612 hydroxides: Cr, Mn, Fe, Co and Ni, Applied Surface Science, 257 (2011) 2717-2730.
- 613 [33] W. Temesghen, P. Sherwood, Analytical utility of valence band X-ray photoelectron
- spectroscopy of iron and its oxides, with spectral interpretation by cluster and band structure
- calculations, Analytical and bioanalytical chemistry, 373 (2002) 601-608.

- 616 [34] L. Hu, A. Khaniya, J. Wang, G. Chen, W.E. Kaden, X. Feng, Ambient Electrochemical
- Ammonia Synthesis with High Selectivity on Fe/Fe Oxide Catalyst, ACS Catalysis, 8 (2018) 9312-
- 618 9319.
- 619 [35] M.W. Louie, A.T. Bell, An investigation of thin-film Ni-Fe oxide catalysts for the
- electrochemical evolution of oxygen, J. Am. Chem. Soc., 135 (2013) 12329-12337.
- 621 [36] A.P. Grosvenor, M.C. Biesinger, R.S. Smart, N.S. McIntyre, New interpretations of XPS
- spectra of nickel metal and oxides, Surface Science, 600 (2006) 1771-1779.
- 623 [37] M.C. Biesinger, L.W.M. Lau, A.R. Gerson, R.S.C. Smart, The role of the Auger parameter in
- XPS studies of nickel metal, halides and oxides, Physical Chemistry Chemical Physics, 14 (2012)
- 625 2434-2442.
- 626 [38] M.C. Biesinger, B.P. Payne, L.W. Lau, A. Gerson, R.S.C. Smart, X-ray photoelectron
- spectroscopic chemical state quantification of mixed nickel metal, oxide and hydroxide systems,
- 628 Surface and Interface Analysis, 41 (2009) 324-332.
- 629 [39] Z. Shi, D. Shi, B. Gao, J. Xu, X. Hu, Z. Wang, Oxidation of Fe-Ni alloys in air at 700 C, 800
- 630 C and 950 C, High Temperature Materials and Processes, 31 (2012) 89-96.
- [40] S.H. Hong, S.H. Ahn, I. Choi, S.G. Pyo, H.-J. Kim, J.H. Jang, S.-K. Kim, Fabrication and
- evaluation of nickel cobalt alloy electrocatalysts for alkaline water splitting, Applied surface
- 633 science, 307 (2014) 146-152.

- 634 [41] K. Duschek, M. Uhlemann, H. Schlörb, K. Nielsch, K. Leistner, Electrochemical and in situ
- magnetic study of iron/iron oxide films oxidized and reduced in KOH solution for magneto-ionic
- 636 switching, Electrochemistry Communications, 72 (2016) 153-156.
- 637 [42] R.S.S. Guzman, J.R. Vilche, A.J. Arvia, The potentiodynamic behaviour of iron in alkaline
- 638 solutions, Electrochimica Acta, 24 (1979) 395-403.
- 639 [43] M. Alsabet, M. Grdeń, G. Jerkiewicz, Electrochemical growth of surface oxides on nickel.
- Part 3: Formation of β-NiOOH in relation to the polarization potential, polarization time, and
- temperature, Electrocatalysis, 6 (2015) 60-71.
- 642 [44] C. Li, J. Hou, Z. Wu, K. Guo, D. Wang, T. Zhai, H. Li, Acid promoted Ni/NiO monolithic
- electrode for overall water splitting in alkaline medium, Science China Materials, 60 (2017) 918-
- 644 928.
- [45] D.S. Hall, C. Bock, B.R. MacDougall, An oxalate method for measuring the surface area of
- nickel electrodes, Journal of The Electrochemical Society, 161 (2014) H787-H795.
- [46] I. Flis-Kabulska, J. Flis, Electroactivity of Ni–Fe cathodes in alkaline water electrolysis and
- effect of corrosion, Corrosion Science, 112 (2016) 255-263.
- 649 [47] L. Ma, Y. Hu, R. Chen, G. Zhu, T. Chen, H. Lv, Y. Wang, J. Liang, H. Liu, C. Yan, Self-
- assembled ultrathin NiCo2S4 nanoflakes grown on Ni foam as high-performance flexible
- electrodes for hydrogen evolution reaction in alkaline solution, Nano Energy, 24 (2016) 139-147.

- [48] X. Wang, C. Xu, M. Jaroniec, Y. Zheng, S.-Z. Qiao, Anomalous hydrogen evolution behavior
- in high-pH environment induced by locally generated hydronium ions, Nature communications,
- 654 10 (2019) 1-8.

- 655 [49] T. Shinagawa, A.T. Garcia-Esparza, K. Takanabe, Insight on Tafel slopes from a microkinetic
- analysis of aqueous electrocatalysis for energy conversion, Scientific Reports, 5 (2015) 13801.
- 657 [50] C. Wei, S. Sun, D. Mandler, X. Wang, S.Z. Qiao, Z.J. Xu, Approaches for measuring the
- surface areas of metal oxide electrocatalysts for determining their intrinsic electrocatalytic activity,
- 659 Chemical Society Reviews, 48 (2019) 2518-2534.
- 660 [51] M.P.M. Kaninski, V.M. Nikolic, G.S. Tasic, Z.L. Rakocevic, Electrocatalytic activation of Ni
- electrode for hydrogen production by electrodeposition of Co and V species, International Journal
- 662 of Hydrogen Energy, 34 (2009) 703-709.
- [52] L. Birry, A. Lasia, Studies of the Hydrogen evolution reaction on raney nickel—molybdenum
- electrodes, Journal of applied electrochemistry, 34 (2004) 735-749.